

Electrical architecture for high power segmented PEM Fuel Cell in vehicle application

*Alexandre De Bernardinis*¹, *Emmanuel Frappé*¹, *Olivier Béthoux*²,
*Claude Marchand*² and *Gérard Coquery*¹

1. IFSTTAR LTN Laboratory of New Technologies / SPEELabs, Versailles Satory, France
e-mails: alexandre.de-bernardinis@ifsttar.fr; emmanuel.frappe@ifsttar.fr; gerard.coquery@ifsttar.fr
2. Laboratoire de Génie Electrique de Paris (LGE) / SPEE-Labs, CNRS UMR 8507; SUPELEC; Université Pierre et Marie Curie Paris VI; Université Paris-Sud XI, Gif-sur-Yvette, France,
e-mails: olivier.bethoux@lgep.supelec.fr; marchand@lgep.supelec.fr

ABSTRACT

In the objective of power increase for transport applications or on-board auxiliaries systems, long fuel cell stacks may be subject to disparities (fluidics, temperature) and can be the cause of possible failures. Coupled with a fault detection strategy, the power converter associated with the fuel cell can act to manage the fault. This article is about power converter topologies applied to a segmented high power fuel cell. The fuel cell generator is a 3-part segmented Polymer Electrolyte Membrane (PEM) fuel cell. Each fuel cell segment can be controlled independently according to its state of health (SoH). The converter topology has to be simple, compact, reliable and with a high efficiency. The resonant isolated boost as converter “technology brick”, allowing soft switching is a candidate topology to meet the technical specifications of the multi-port fuel cell-converter system.

Index Terms— Fault detection strategy, multi-port converter, power conditioning, resonant isolated boost, segmented PEM fuel cell

1. INTRODUCTION

The electric vehicle (EV) is an environment-friendly mean of transportation in the sense where it has a “locally” clean energy. A possible electric generator is the fuel cell (FC) PEMFC technology with proton exchange membrane; it then should be of sufficient power level for the drive of the vehicle. The power increase of fuel cells is achieved by long stacks of cells units (> 100) as well as by an increase of their active surface. Nevertheless the increase of the number of cells is limited by mechanical constraints and waterproofness of cell units [1]. Moreover a large number of cells or a too wide active surface makes the fluidic management of the fuel cell difficult, so disparities in the reactant gas supply can appear within a cell [2, 3] or between them [4-6]. It results a non-uniformity between the cell voltages [7] and a possible appearance of defects of type flooding or drying [8, 9]. Therefore, the use of several fuel cell stacks allows an increase of power while using standard-technology modules which their size and their management are easier. It is the “multi-stack association concept”, already presented in [10, 11]. Besides, a disparity of temperature throughout the stack makes that flooding mainly appears on the extremities of the stack, where the temperature is lower, and drying takes place rather in the center of the fuel cell where the temperature

is higher [12-16]. Thus, during the appearance of a defect, which can only affect some cells, a corrective action must be taken on the whole stack including also the healthy cells. A fluidic action based on fuel cell conditioning auxiliaries (air compressor, humidifier, temperature regulation) is already a solution. However, for long stacks, faults can appear on localized areas, mainly affecting some cells or groups of cells [17]. Then, the fluidic circuitry may become complex to be used in case of fault appearance. In this paper, electrical power conditioning is explored as a new corrective action. For this purpose, power converters can be considered either as a global electrical interface for the FC generator or can act on localized areas of the stack. Indeed, as fuel cell voltage significantly varies according to power, these converters are naturally present in a fuel cell system to regulate the load voltage. Considering the fact that faults will mainly affect some particular cells or groups of cells, localized power converter architecture will be rather explored. The associated electric architecture should be simple, economic, and reliable and should have high energy efficiency, such as not to penalize the nominal functioning. The schedule of the communication is as follows: We start first with the presentation of a fault detection strategy for PEM fuel cell, then we discuss the respective interests of the AC and the DC couplings for the power transfer between the fuel cell generator and the

load. For the DC-link power transfer, four isolated topologies will be studied. The result of a comparative study will bring us to define the global multi-port electrical architecture, the associated DC-bus voltage regulation and the technology to realize the converter.

2. FEEDBACK ON THE FAULT DETECTION STRATEGY FOR PEM FUEL CELL

A fault detection strategy has been proposed by Frappé *et al.* in [17]. It basically relies on voltage measurement and intends to make use of the small disparity of temperature as well as the non-uniform distribution of reactants along the stack. The fact is that many authors pointed out the cell discrepancies throughout the stack which depend on the operating conditions [4]. Some authors observed that cell voltage is lower in the cells furthest from the fuel inlet of the stack (nearest to the air inlet) due to uneven gas distribution or water flooding [16]. Different experiments also point out that the central region of the stack is hotter than its exterior and subsequently drying mostly occurs in center cells [14, 15]. In fact, Ramousse *et al.* [12] highlights that water in the cells is highly dependent on the temperature; as a result flooding occurs in cooler cells and drying in hotter cells. Based on these remarks, we suggest measuring the voltage of group of cells in the inlet, the center and the outlet of the stack (Figure 1).

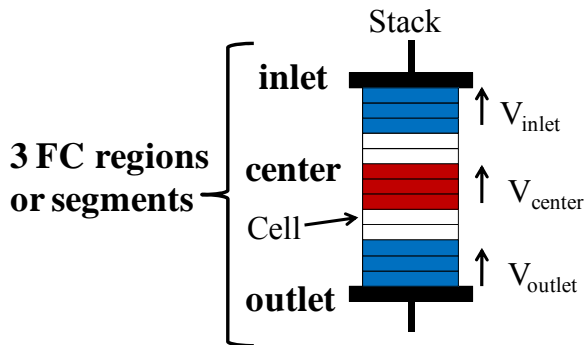


Figure 1. Principle of monitoring group of cells for a PEM fuel cell stack.

It appears relevant to instrument with voltage sensors three main areas of the stack: the inlet, the outlet and the center. In this case, the detection principle is based on the monitoring of a differential between the voltage in the center of the stack (V_{center}) and the inlet/outlet voltages (resp. V_{inlet} , V_{outlet}). This principle allows generating a new state-of-health indicator of the fuel cell stack. In the case of no fault, all voltages are constant or drop similarly due to load variation: the differential equals zero. If a drying appears, only V_{center} drops and the two differential voltages become positive. However, if a flooding occurs, the inlet and/or the outlet voltage drop leading to a decrease of one or two differential voltages. Using the differential method, the FC stack can be

assimilated to a voltage sensor. Its characteristic is to provide two key signals representative of the state of health. The feedback information is simple, fast and based on the real-time operating conditions without adding any external disturbance. Moreover the method can be applied also when the operating conditions are slightly modified.

3. STUDY OF CONVERTER TOPOLOGIES FOR THE POWER TRANSFER

Power transfer between different fuel cell segments and the load can be achieved via two types of electrical links: one AC-link or a DC-link. AC-link authorizes directly the power transfer through the transformer, for example thanks to the use of a multi windings transformer. DC-link imposes an indirect conversion type as “inverter-isolation-rectifier”, but permits to regulate easily the power between the different segments thanks to the DC node. Figures 2 and 3 illustrate the principle of power transfer using AC and DC-link.

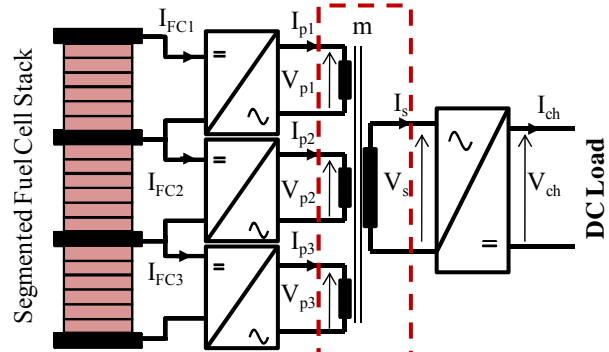


Figure 2. Electrical architecture with AC-link.

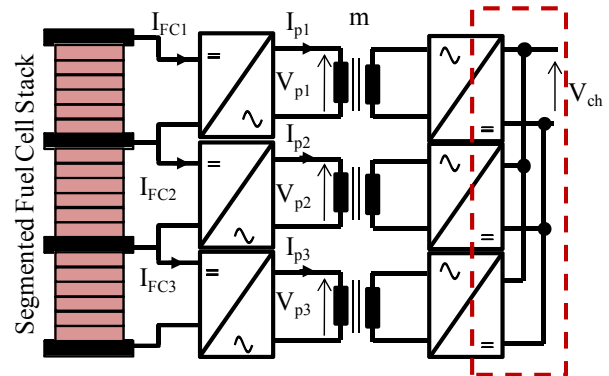


Figure 3. Electrical architecture with DC-link.

Technical specifications: The 30kW fuel cell generator is subdivided into 3 equal parts of 10kW, 200 cm² of active area, 100 cells.

- No-load voltage: 100V
- Nominal current : 166 A
- Voltage at nominal load: 60V

The power converter is able to regulate the output power to 540 VDC, which value is a standard in railways and heavy land vehicles. The following study is focalized on one “converter brick” associated to one fuel cell segment.

3.1 Power transfer through the AC-link (or AC node)

The segmented concept for the fuel cell implies the use of insulation between the segments; a first approach has concerned the possibility of using the AC-link for the power transfer. Some research works have already been published on the topic [18-22]. Each port of the transformer is connected to a voltage source inverter which delivers a rectangular shaped voltage (-V, 0, +V). The power transfer between two ports is achieved thanks to a voltage shift. The leakage inductance L_k and switching frequency interfere also in the power transfer adjustment (Figures 4 and 5). This topology allows an effective regulation of the power between different ports.

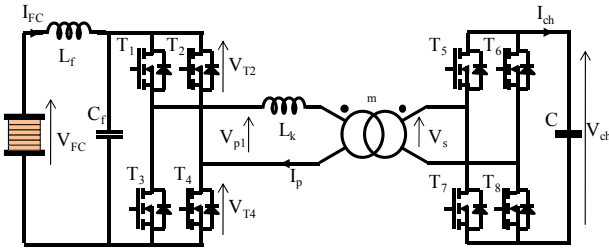


Figure 4. AC-link: Phase-shifted inverter topology.

Moreover, authors have proposed a control methodology which is able to decouple the energy fluxes issued from each converter. In order to achieve this properly, output AC voltage (V_s) and current (I_s) are set in phase. In order to reduce switching losses, and taking into account the proposed control strategy, a zero voltage switching (ZVS) mode is possible. This strategy has been proposed in [18].

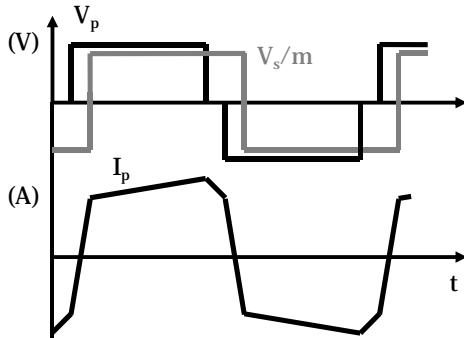


Figure 5. Phase-shifted inverter topology: Typical waveforms.

However, the phase-shifted inverter topology is optimal only when the AC voltages V_p and V_s/m have the same amplitude, so in the absence of phase-shift no current circulates through the leakage inductance L_k . This topology is thus very sensitive to the variations of the FC input voltage, which are going to engender a reactive

current which can be important within the AC link. Furthermore, because of the structure of voltage inverter, there is a presence of a strong AC ripple which can impact on the fuel cell. The use of an input filter is then imperative, but will contribute to increase the size of the converter. Hence, the use of the AC-link is not recommended namely because of the electrical characteristics of the fuel cell. For this reason, another type of electrical coupling is envisaged.

3.2 Power transfer through the DC-link (or DC node)

We focus in this section on the power transfer through the DC-node. The starting point of the study is the Boost converter which is composed of a reduced number of controlled switches. It has a high efficiency and the possibility of reducing current constraints thanks to the interleaving technique. Furthermore, a Boost topology allows controlling the FC input current, so transient current can be imposed and current ripple limited thanks to the input inductance. Such a Boost converter topology is thus well adapted to the fuel cell dynamic behavior.

3.2.1. Half bridge isolated boost

The isolated boost is derived from a 2-leg interleaved boost on which is added a galvanic insulation by transformer between inductances-transistors and rectifier diodes [23] (Figure 6). The control orders for the switches are identical and π shifted. Its voltage ratio corresponds to that of the boost added with transformer ratio m : $V_{ch} = \frac{m}{1-\alpha} V_{FC}$

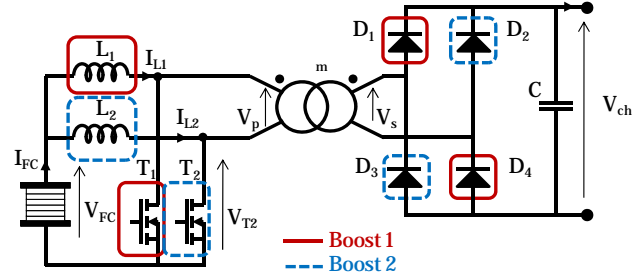


Figure 6. Half-bridge isolated Boost.

Due to its design principle a working with a duty-cycle α lower than 0.5 is forbidden, which implies that the voltage across the switches is at least $V_{FC} \times 2 = 200V$. The electric constraints on semiconductor switches, with a transformer ratio $m = 2.5$, inductances $L1=L2= 165\mu H$, and a switching frequency $f=10$ kHz are:

$$V_{T \max} = \frac{V_{ch}}{m} = 216V \quad V_D = V_{ch} = 540V$$

$$I_{T \max} = I_{FC} + \frac{(2-\alpha)V_s(1-\alpha)}{2mL_1f} = 168A$$

$$I_{D \max} = \frac{I_{FC}}{2m} + (1-\alpha)^2 \frac{V_s}{2m^2L_1f} = 37A$$

The disadvantages of this structure are the impossibility to operate with a duty-cycle lower than $\frac{1}{2}$, which implies a rather high voltage caliber for semiconductor devices. That is the reason why another isolated topology (full bridge isolated boost) is studied which allows reducing the voltage constraint on switches placed at the primary of the transformer.

3.2.2. Full bridge isolated boost

A full-bridge isolated boost structure isolated is presented in [24] (Figure 7). The control order for the switches is identical to the previous topology and its voltage ratio is: $V_{ch} = \frac{m}{1-D} V_{FC}$ With $D = 2\alpha - 1$, the duty-cycle seen by the input inductance L . α is the duty-cycle of the control orders of switches. Thus, although α has always to be higher than $\frac{1}{2}$, from the input inductance side, the boost operates with a duty cycle D ranging from 0 to 1. We can then use the boost over all its operating range and not only the half range as for the previously studied half-bridge isolated boost.

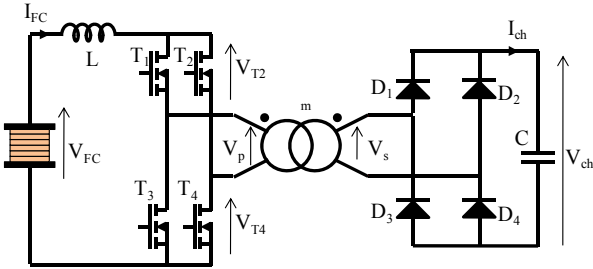


Figure 7. Full-bridge isolated Boost.

The voltage constraints on switches are consecutively divided by two. With a transformer ratio equal to $m=5$, an inductance $L=86\mu\text{H}$, these constraints become:

$$V_{T \max} = \frac{V_{ch}}{m} = 110V \quad V_D = V_{ch} = 540V$$

$$I_{r \max} = I_{FC} + \frac{(2\alpha - 1)V_s(1 - \alpha)}{m L f} = 180A$$

$$I_{D \max} = \frac{I_{FC}}{m} + (1 - \alpha)^2 \frac{2V_s}{m^2 L f} = 37A$$

However, these two isolated boost topologies operating on hard switching require, because of the leakage inductance of the transformer, a clamping circuit during the opening of switches. This clamping circuit can be active by the addition of a capacity and a switch [25] or passive by the addition of a diode, a capacity and a resistance [27]. Nevertheless, for both cases, the losses of the converter are increased. Another possibility is to make the MOSFETs operate in avalanche mode, the resulting avalanche energy is then transferred into the switches and no additional element is required [26]. In order to use the MOSFETs in avalanche, it is necessary to make sure that

the leakage inductance L_k of the transformer is the smallest possible and the sizing of heat sink should take into account this functioning which is severe for switches. Hence, to make sure to minimize at most the losses of the converter, a third topology is studied. It operates using soft switching to minimize the switching losses.

3.2.3. Resonant isolated boost

This structure is presented by [27-30] (Figure 8). A capacitor C_p is added to establish a quasi-resonant circuit with the leakage inductance L_k . Thus, this structure is not subject to voltage peaks due to the opening (switch-off) of semiconductor switches. The resonant circuit allows obtaining a working at zero current switching (ZCS) (Figure 9).

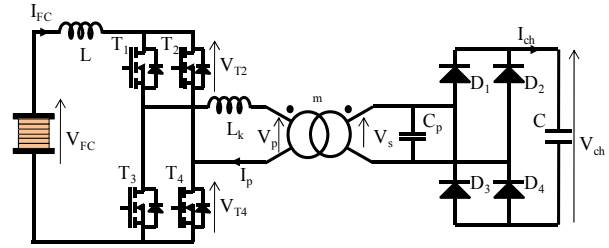


Figure 8. Resonant isolated Boost topology.

The converter control is now realized by frequency tuning. In steady states, the load voltage – FC voltage

$$\text{relation is given by: } V_{ch} = \frac{m}{1 - \frac{f}{f_r}} V_{FC}$$

This equation shows that the converter frequency control significantly evolves according to FC voltage variation. Namely, considering a fixed output voltage (V_{ch}) and a $[V_{FC}/2; V_{FC}]$ FC voltage range, the control frequency varies from f_{min} to $f_{max} = 2.5 f_{min}$. Moreover, over the whole converter working range, the ZCS mode has to be validated.

The converter operating frequency is chosen between 17 kHz and 38 kHz; f_{max} corresponds to the maximal current. These frequency values are a trade-off between acceptable losses for the semiconductors and size of the high frequency transformer. Resonant circuit parameters are L_k

$$= 1.62\mu\text{H} \text{ and } C_p = 2.61\mu\text{F}; f_r = \frac{1}{2\pi\sqrt{L_k C_p}} = 78 \text{ kHz is}$$

the resonant frequency. Selecting a transformer ratio $m=4$, an inductance $L=38\mu\text{H}$, the switches constraints are computed as follows:

$$V_{T \max} = \frac{V_{ch}}{m} = 135V \quad I_{T \max} = \frac{V_s}{m\sqrt{\frac{L_k}{C_p}}} = 170A$$

$$V_D = V_{ch} = 540V \quad I_{D \max} = \frac{I_{FC}}{m} = 40A$$

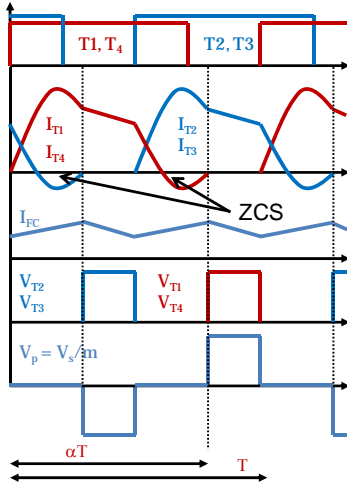


Figure 9. Resonant isolated Boost topology: Typical waveforms.

3.2.4. Double resonant inverter topology

A voltage source inverter (VSI) topology with double resonance [31], already studied at IFSTTAR LTN for an application of battery charger for shunting locomotive [32] is presented in Figure 10. This structure also allows an operation in ZCS and is compared with the previous current-fed resonant structure. The working of the converter is obtained between two characteristic frequencies: the minimal frequency (or anti-resonance) for which the converter does not deliver any current and the resonance frequency for which the current amplitude is maximal. It is possible to limit the functioning of the converter between these two frequencies. Nevertheless, the transformer ratio is high using this structure ($m=11$). Moreover, the current constraints on switches are important and depend on resonant parameters: $L_s = 0.2\mu\text{H}$, $L_p = 4.2\mu\text{H}$, $C_p = 14.7\mu\text{F}$, $F_r = 83\text{kHz}$. This topology also requires an input filter for attenuating the FC current undulation.

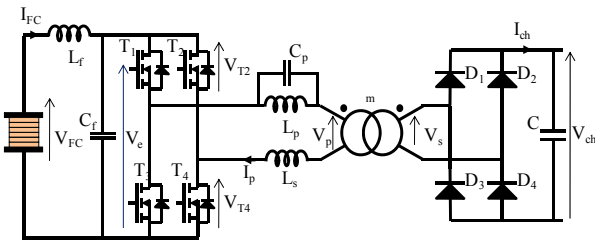


Figure 10. Double resonant inverter topology.

$$V_{T\max} = \frac{V_{ch}}{m} = 50V \quad I_{T\max} = I_{FC} + \frac{V_{ch}}{m Z_r} = 550A$$

With Z_r the resonant impedance: $Z_r = \sqrt{\frac{L_s}{C_p}}$

$$V_D = V_{ch} = 540V, \quad I_{D\max} = \frac{I_{T\max}}{m} = 50A$$

3.3. Quantification of efficiencies

The different presented topologies have been simulated and compared in terms of global efficiency. Simulations and numerical calculation of efficiencies have been performed using Matlab-Simulink[®]. Specific parameters for the semiconductor devices have been addressed using technical datasheets. Boost-based topologies permit to control the input current, and are well suited for the electrical coupling with a fuel cell. On the contrary inverter-based (phase-shifted) topologies lead to an input fuel cell current which presents an AC ripple and may be discontinuous. This constraint imposes to add an input filter. Efficiencies versus FC current for the 5 studied converters are summarized in Figure 11.

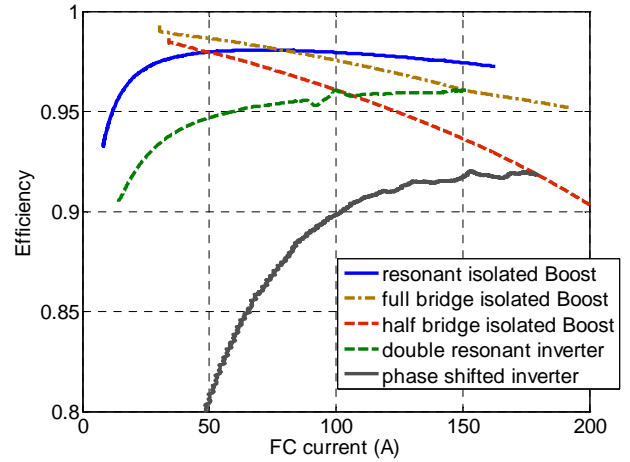


Figure 11. Efficiency of studied power converters.

The resonant isolated boost offers the best performances for a FC current amplitude higher than 80A, in contrary to hard-switching topologies for which the efficiency decreases rapidly. It has the advantage to allow a working of the switches less severe (soft-switching) than hard-switched isolated boost which operates during avalanche. It is composed of the same number of semiconductors than the full-bridge isolated boost. The resonant circuit is composed of the transformer leakage inductance, and only one added capacitance is required.

As a consequence, the resonant isolated boost is a candidate topology for the technical specifications, and will be defined as the “converter brick” for the global “multi-port fuel cell-converter” system.

3.4. Simulation results for the resonant isolated boost

Simulation results using Matlab-Simulink[®] software tool are presented for the resonant isolated boost converter. Matlab-Simulink[®] has been chosen rather than other electric circuit software existing on the market. Indeed, the Simulink interface permits to easily couple power converter block models with the associated control strategy in the same workspace and is linked with the Matlab[®] workspace for numerical calculations. They

illustrate respectively the evolution of the fuel cell power versus the converter frequency (Figure 12); focus on resonant current, fuel cell current ripple rate for 120A (Figure 13) and load variations with DC bus voltage regulation performance (Figure 14). FC current, voltage and DC bus voltage (540V) are correctly controlled for both permanent and transient regimes.

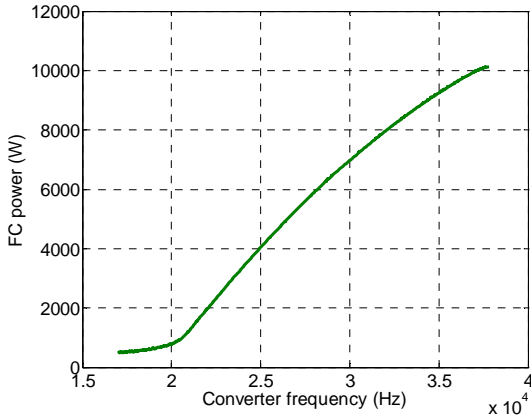


Figure 12. FC power (W) vs converter frequency (Hz).

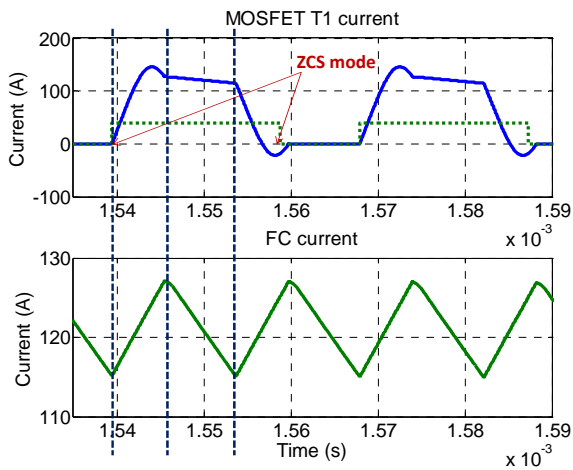


Figure 13. Focus on resonant and FC ripple currents (A).

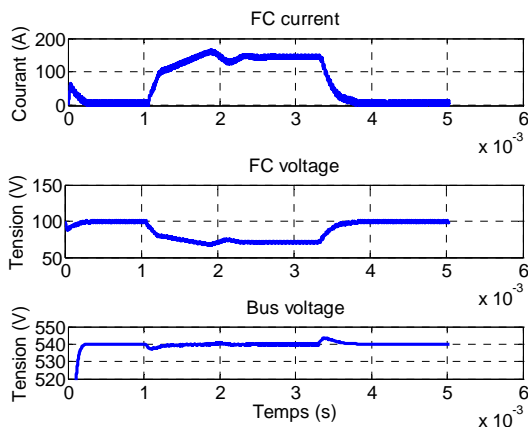


Figure 14. Load variations (+ zoom on the regulated 540V DC bus voltage).

4. GLOBAL ELECTRICAL ARCHITECTURE - VOLTAGE REGULATION AND TECHNOLOGY

The resonant isolated boost is adopted in order to realize the converter system associated to the 3-part segmented PEM fuel cell. Output voltage regulation is performed thanks to 2 regulation loops. The outer loop, for the voltage regulation, is common to all the system. The current reference I_{ref} calculated by the PI voltage controller is shared between the 3 converters. Each input converter has its own inner loop for fuel cell current control. Figure 15 shows the global synoptic of the system regulation. In addition the supervisor's role has to manage the power distribution (dispatching) between inputs according to the FC segment state of health. Figure 16 presents the voltage and current regulation strategy. Each converter can be controlled independently. The output of the PI voltage controller constitutes the current reference for the 3 FC segments (I_{FC1} , I_{FC2} , I_{FC3}). Their comparison with measured current values generates each frequency reference value (f_{ref1} , f_{ref2} , f_{ref3}) for the converters.

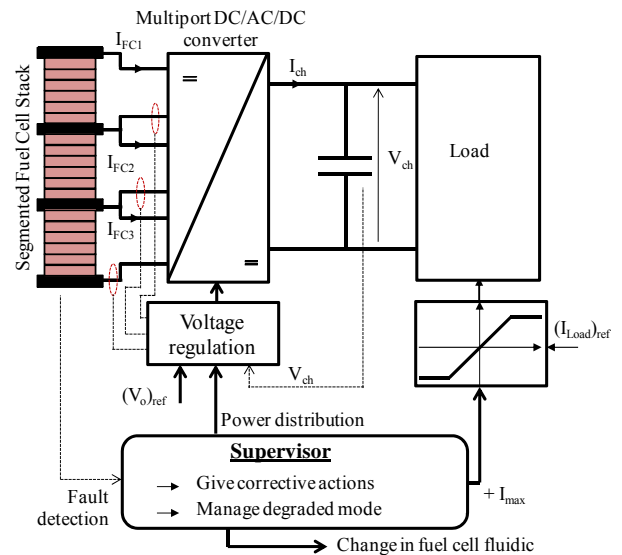


Figure 15. Synoptic of the multi-port system regulation.

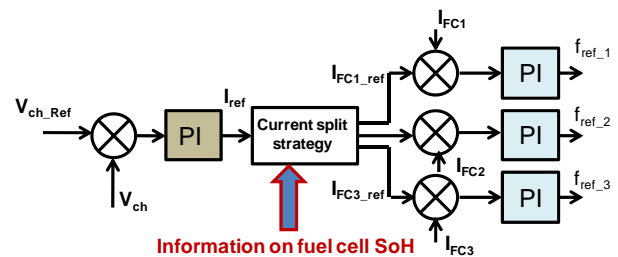


Figure 16. Voltage and current regulation strategy.

The use of high frequencies (20 to 40 kHz range) permit to select a planar technology for the transformer, which leads to a compact solution. The transformer should be

designed by the Payton company [33] with the desired characteristics: 10kW output power, primary/secondary voltage 135/540V, primary/secondary current 170/40A and a leakage inductance equals to 160 μ H. Primary transformer voltage is low (135V), so HiPerFET™ MOSFETs technology from IXYS are chosen [34]. They offer a low on-state $R_{DS(ON)}$ resistance. Selected capacitances are medium power film capacitors from AVX, especially chosen for DC filtering. Finally, the input inductance L is designed for 38 μ H for a maximal current of 160A and +/- 10% of current ripple (Table 1).

Table 1. Technology for the resonant isolated boost.

	Constraints devices caliber	Technological choice
Input inductance : L	38 μ H, 160A $\Delta I = \pm 10\%$ ($\pm 16A_{max}$)	Ferrite / Iron powder cores
MOSFETs: T ₁ to T ₄	135V – 170A	2 MOSFETs in parallel IXYS IXFN210N20P 200V-188A [34]
HF Transformer	135 – 540V, 170 – 40A, m = 4; 10kW	Planar technology transformer from “Payton planar Magnetics” [33]
Resonant capacitor : C _p	2.61 μ F, 540V – 40A _{max}	4 capacitors in series TPC- AVX FFV36C0136K 150Vrms – 25A _{rms}
Rectifier diode bridge : D ₁ to D ₄	540V – 40A	DSEP2x91-06A – 600V – 90A
DC bus capacitor : C	50 μ F, 540V – 20A	FFG86K0586K – 600V – 44A – 56 μ F

5. CONCLUSION

The segmented concept associates both compactness of one single fuel cell and the potentialities of “modularity” of a “multi-stack” system. However, this configuration doesn’t allow acting independently on the fluidic of each segment, which can be compensated by an electric action. The resonant isolated boost offers the best energetic efficiency among all the studied converter topologies. Its working allowing soft switching (ZCS) permits to minimize the solicitations on the semiconductors by canceling the switching losses. Efficiency is an important criterion for the global multi-port converter system because of the necessity of one converter per segment. Each “converter brick” is independent and can act on the corresponding FC segment, thanks to a dedicated control strategy. Technology choices are also important in order to ensure a compact (high power density) integrated power converter structure with improved efficiency and compatible with vehicle requirements.

6. REFERENCES

- [1] P. Lin, P. Zhou, and C. W. Wu, “A high efficient assembly technique for large PEMFC stacks,” *Journal of Power Sources*, vol. 194, no. 1, pp. 381-390, Oct. 2009.
- [2] S. G. Kandlikar, Z. Lu, T. Y. Lin, D. Cooke, and M. Daino, “Uneven gas diffusion layer intrusion in gas channel arrays of proton exchange membrane fuel cell and its effects on flow distribution,” *Journal of Power Sources*, vol. 194, no. 1, pp. 328-337, Oct. 2009.
- [3] S. G. Kandlikar, Z. Lu, W. E. Domigan, a D. White, and M. W. Benedict, “Measurement of flow maldistribution in parallel channels and its application to ex-situ and in-situ experiments in PEMFC water management studies,” *International Journal of Heat and Mass Transfer*, vol. 52, no. 7-8, pp. 1741-1752, Mar. 2009.
- [4] M. Miller and A. Bazylak, “A review of polymer electrolyte membrane fuel cell stack testing,” *Journal of Power Sources*, vol. 196, no. 2, pp. 601-613, Jan. 2011.
- [5] P. A. C. Chang, J. St-Pierre, J. Stumper, and B. Wetton, “Flow distribution in proton exchange membrane fuel cell stacks,” *Journal of Power Sources*, vol. 162, no. 1, pp. 340-355, Nov. 2006.
- [6] R. Mustata, L. Valiño, F. Barreras, M. I. Gil, and A. Lozano, “Study of the distribution of air flow in a proton exchange membrane fuel cell stack,” *Journal of Power Sources*, vol. 192, no. 1, pp. 185-189, Jul. 2009.
- [7] J. Park and X. Li, “Effect of flow and temperature distribution on the performance of a PEM fuel cell stack,” *Journal of Power Sources*, vol. 162, no. 1, pp. 444-459, Nov. 2006.
- [8] X. Liu, H. Guo, F. Ye, and C. Ma, “Water flooding and pressure drop characteristics in flow channels of proton exchange membrane fuel cells,” *Electrochimica Acta*, vol. 52, no. 11, pp. 3607-3614, 2007.
- [9] F. Weng, a Su, and C. Hsu, “The study of the effect of gas stoichiometric flow rate on the channel flooding and performance in a transparent fuel cell,” *International Journal of Hydrogen Energy*, vol. 32, no. 6, pp. 666-676, May 2007.
- [10] A. De Bernardinis, M.-C. Péra, J. Garnier, D. Hissel, G. Coquery, and J.-M. Kauffmann, “Fuel cells multi-stack power architectures and experimental validation of 1kW parallel twin stack PEFC generator based on high frequency magnetic coupling dedicated to on board power unit,” *Energy Conversion and Management*, vol. 49, no. 8, pp. 2367-2383, 2008.
- [11] B. Vulturescu, A. De Bernardinis, R. Lallemand, and G. Coquery, “Traction power converter for PEM fuel cell multi-stack generator used in urban transportation,” in Proc. European Conference on Power Electronics and Applications, Aalborg Denmark, September 2007, CD-Rom pp. 1-10.
- [12] J. Ramousse, K.P. Adzaka, Y. Dubé, K. Agbossou, M. Fournier, A. Poulin, and M. Dostie, “Local Voltage Degradations (Drying and Flooding) Analysis Through

- 3D Stack Thermal Modeling,” *Journal of Fuel Cell Science and Technology*, vol. 7, 2010, p. 041006.
- [13] A. Hernandez, R. Outbib, and D. Hissel, “Diagnostic d’une pile à combustible PEMFC. Une approche statistique,” *Journal Européen des Systèmes Automatisés*, vol. 42, no. 10, pp. 1225-1277, 2008.
- [14] J. Jang, H. Chiu, W. Yan, and W. Sun, “Effects of operating conditions on the performances of individual cell and stack of PEM fuel cell,” *Journal of Power Sources*, vol. 180, no. 1, pp. 476-483, May 2008.
- [15] R. Eckl, W. Zehntner, C. Leu, and U. Wagner, “Experimental analysis of water management in a self-humidifying polymer electrolyte fuel cell stack,” *Journal of Power Sources*, vol. 138, no. 1-2, pp. 137-144, Nov. 2004.
- [16] W. H. Zhu, R. U. Payne, D. R. Cahela, and B. J. Tatarchuk, “Uniformity analysis at MEA and stack Levels for a Nexa PEM fuel cell system,” *Journal of Power Sources*, vol. 128, no. 2, pp. 231-238, Apr. 2004.
- [17] E. Frappé, A. De Bernardinis, O. Bethoux, D. Candusso, F. Harel, C. Marchand and G. Coquery, “PEM fuel cell fault detection and identification using differential method: simulation and experimental validation,” *Eur. Phys. J. Appl. Phys.* 54, 23412 (2011).
- [18] E. Frappé, A. De Bernardinis, O. Bethoux, C. Marchand, and G. Coquery, “A Soft-Switching Multisource DC-DC Converter for Segmented PEM Fuel Cell Power Management in Vehicle Application,” in Proc. IEEE Vehicle Power and Propulsion Conference, Chicago, September 2011.
- [19] S. Mariethoz and A. Rufer, “Multisource DC-DC converter for the supply of hybrid multilevel converter,” Conference Record of the 2006 IEEE Industry Applications Conference Forty-First IAS Annual Meeting, vol. 2, no. c, pp. 982-987, Oct. 2006.
- [20] N. Schibli, “DC-DC converters for two-quadrant operation with controlled output voltage,” in Proc. EPE 99, Lausanne, September 1999, pp. 1-7.
- [21] F. Krismer, S. Round, and J. Kolar, “Performance optimization of a high current dual active bridge with a wide operating voltage range,” in Proc. Power Electronics Specialists Conference, PESC’06. 37th IEEE, 2006, vol. pp, pp. 1-7.
- [22] C. Zhao, S. D. Round, and J. W. Kolar, “An isolated three-port bidirectional DC-DC converter with decoupled power flow management,” *Power Electronics, IEEE Transactions on*, vol. 23, no. 5, pp. 2443-2453, Sep. 2008.
- [23] Y. Lembeye, V. D. Bang, G. Lefevre, and J.-P. Ferrieux, “Novel Half-Bridge Inductive DC-DC Isolated Converters for Fuel Cell Applications,” *IEEE Transactions on Energy Conversion*, vol. 24, no. 1, pp. 203-210, Mar. 2009.
- [24] M. Nyman and M. A. E. Andersen, “High-Efficiency Isolated Boost DC-DC Converter for High-Power Low-Voltage Fuel-Cell Applications,” *IEEE Transactions on Industrial Electronics*, vol. 57, no. 2, pp. 505-514, Feb. 2010.
- [25] A. Vazquez, C. Aguilar, and F. Canales, “Comparison between two-stage and integrated power conditioner architecture for fuel cell based power supply system,” in Power Electronics Congress, 2008, CIEP 2008. 11th IEEE International, 2008, pp. 177-184.
- [26] K. Wang, C. Y. Lin, L. Zhu, D. Qu, F. C. Lee, and J. S. Lai, “Bi-directional DC to DC converters for fuel cell systems,” in *Power Electronics in Transportation*, 1998, 1998, pp. 47-51.
- [27] H. Benqassmi, J.-P. Ferrieux, and J. Barbaroux, “Current-source resonant converter in power factor correction,” in Proc. PESC97. Record 28th Annual IEEE Power Electronics Specialists Conference., 1997, pp. 378-384.
- [28] J.-F. Chen, R.-Y. Chen, and T.-J. Liang, “Study and Implementation of a Single-Stage Current-Fed Boost PFC Converter With ZCS for High Voltage Applications,” *IEEE Transactions on Power Electronics*, vol. 23, no. 1, pp. 379-386, Jan. 2008.
- [29] R. Y. Chen, R. L. Lin, T. J. Liang, J. F. Chen, and K. C. Tseng, “Current-fed full-bridge boost converter with zero current switching for high voltage applications,” Fortieth IAS Annual Meeting. Conference Record of the 2005 Industry Applications Conference, 2005., pp. 2000-2006, 2005.
- [30] R.-Y. Chen, T.-J. Liang, J.-F. Chen, R.-L. Lin, and K.-C. Tseng, “Study and Implementation of a Current-Fed Full-Bridge Boost DC-DC Converter With Zero-Current Switching for High-Voltage Applications,” *IEEE Transactions on Industry Applications*, vol. 44, no. 4, pp. 1218-1226, 2008.
- [31] V. Croulard, G.-W. Baptiste, and A. Durville, “Double resonance electronic converter,” U.S. Patent 2003023151428-Apr-2003.
- [32] A. De Bernardinis, S. Butterbach, R. Lallemand, A. Jeunesse, G. Coquery, and P. Aubin, “Double resonant converter topology with fast switching semiconductors for lead-acid battery charger used in hybrid electric locomotive,” in Proc. 2011 IEEE International Symposium on Industrial Electronics, Gdansk Poland, June 2011, pp. 239-244.
- [33] P. Špánik, I. Feňo, G. Kácsor, I. Lokšeninec, “Using planar transformers in soft-switching DC-DC power converters,” *Application Note*, consulted online 1st February 2012 at: http://www.paytongroup.com/info/Planar%20trans._pa_per.pdf.
- [34] Tech. Datasheet: IXFN210N20P, IXYS Corp. 2010.